TISSUE ENGINEERING: Part A
Volume 21, Numbers 3 and 4, 2015

DOI: 10.1089/ten.tea.2014.0250

Engineered Microporosity: Enhancing the Early Regenerative Potential of Decellularized Temporomandibular Joint Discs

Cassandra M. Juran, PhD,[1] M. Franklin Dolwick, DMD, PhD,[2] and Peter S. McFetridge, PhD[1]

The temporomandibular joint (TMJ) disc is susceptible to numerous pathologies that may lead to structural degradation and jaw dysfunction. The limited treatment options and debilitating nature of severe temporomandibular disorders has been the primary driving force for the introduction and development of TMJ disc tissue engineering as an approach to alleviate this important clinical issue. This study aimed to evaluate the efficacy of laser micropatterning (LMP) *ex vivo*-derived TMJ disc scaffolds to enhance cellular integration, a major limitation to the development of whole tissue implant technology. LMP was incorporated into the decellularized extracellular matrix scaffold structure using a 40 W CO_2 laser ablation system to drill an 8×16 pattern with a bore diameter of 120 μm through the scaffold thickness. Disc scaffolds were seeded with human neonatal-derived umbilical cord mesenchymal stem cells differentiated into chondrocytes at a density of 900 cells per mm^2 and then assessed on days 1, 7, 14, and 21 of culture. Results derived from histology, PicoGreen DNA quantification, and cellular metabolism assays indicate that the LMP scaffolds improve cellular remodeling compared to the unworked scaffold over the 21-day culture period. Mechanical analysis further supports the use of the LMP showing the compressive properties of the LMP constructs closely represent native disc mechanics. The addition of an artificial path of infiltration by LMP culminated in improved chondrocyte adhesion, dispersion, and migration after extended culture aiding in recapitulating the native TMJ disc characteristics.

Introduction

The temporomandibular joint (TMJ) is a mechanically active joint consisting of the articulating structures of the mandible and the temporal bone of the skull (Fig. 1A, B). These skeletal components are highly incongruent lending to complex mechanical loading that is disseminated through a cartilaginous biconcave disc located between the mandible's condyle and glides along the temporal bone's glenoid fossa and articular eminance.[1] Joint movements involved in facial expressions, talking, drinking, and eating impose compressive, shear, tensile, and rotational forces on the joint, indicating that the disc possesses a high degree of mechanical resilience.[2–4]

Severe degeneration or damage of the TMJ disc requiring surgical removal of the disc (discectomy) often leaves a patient suffering from, or vulnerable to, painful jaw locking, osteoarthritis, or bone degeneration. This leads to additional damage to the articulating skeletal structures, which further exacerbates the aforementioned symptoms and dysfunction.[5–7] Current approaches to develop functional TMJ disc replacements have utilized synthetic materials (Proplast Teflon), a variety of self-assembly gels (PEG, PLLA, collagen matrix), and autologous implants (fat implants or muscle lips). These methods have seen limited clinical success with outcomes often resulting in encapsulation, fragmentation, and degeneration that are likely due to mechanical and/or biochemical incompatibility.[8–11]

Decellularized naturally derived scaffolds have been shown to retain native biochemistry, microenvironmental architecture, and mechanical properties of the native tissues they are derived from.[12,13] Specifically, the use of the surfactant sodium dodecyl sulfate (SDS) to decellularize TMJ discs has resulted in scaffolds, which retain the mechanical integrity and molecular architecture of the native TMJ disc.[14] However, a major limitation with the use of many naturally derived scaffolds is that cell ingrowth is restricted by the dense fibril microenvironment (collagen, elastin, glycosaminoglycan [GAG]), and inherit lack of a microvasculature to support cell function.[15,16]

The goal of these investigations was to employ a processing technique using carbon dioxide laser micropatterning (LMP) to modify the dense micro architecture of the TMJ disc to increase cellular integration and improve mass

[1]J. Crayton Pruitt Family Department of Biomedical Engineering, University of Florida, Gainesville, Florida.
[2]Division of Oral and Maxillofacial Surgery, College of Dentistry, University of Florida, Gainesville, Florida.

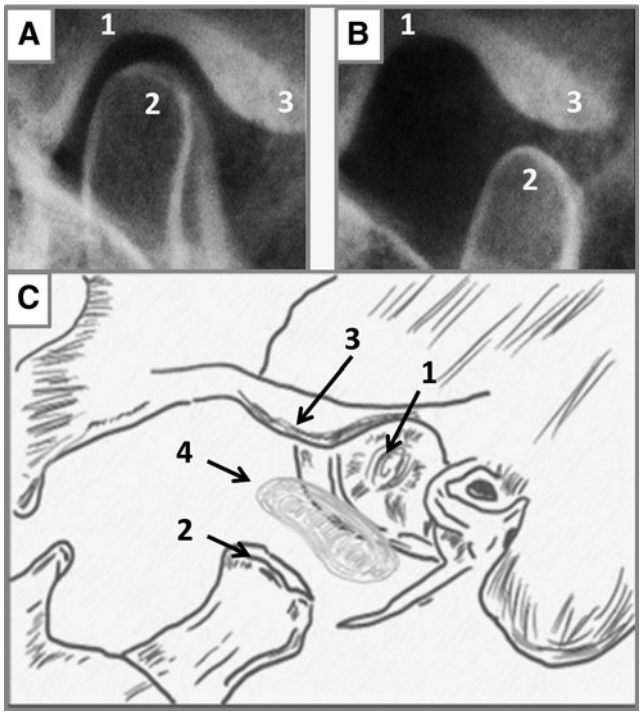

FIG. 1. Temporomandibular joint (TMJ) anatomy and joint articulation. **(A, B)** The articulation of the mandibular condyle within the infratemporal fossa while **(C)** is an expanded illustration of the major skeletal connections of the TMJ and the articulating disc. (1) Articular fossa, (2) mandibular condyle, (3) articular eminence, and (4) TMJ fibrocartilage disc.

transport during initial remodeling. To control uniformity of the laser micropatterning, the acellular scaffold was lyophilized (freeze-dried) before laser working to eliminate laser spread (refraction, reflection, thermal conductivity) associated with hydrated tissue.[17,18]

CO_2 laser ablation of biological material has been shown to be effective, inexpensive, and allows precise and repeatable method to control pore geometry. A consideration with CO_2 laser ablation is the spot size, dictated by the wavelength (10.6 μm), which limits the minimum beam width to ~80 μm. Murphy *et al.* evaluated cell adhesion and proliferation as a function of pore size (85–325 μm) and found that a mean pore size of 120 μm enhanced for initial cell attachment and proliferation (48 h).[19–21] Thus, the spot size using this approach falls within the optimum window for cellular integration. Other laser ablation studies performed on biomimetic gels have shown that the incorporation of laser ablated pores enhances cellular infiltration. The major differences between previous studies and these investigations are these works ablate a natural extracellular matrix (ECM) material, which retains biochemical and biomechanical properties of the target tissue. In addition, these works ablate through a tissue >2 mm in thickness while previous studies have been limited to less than 1 mm thickness.[22–24]

An ideal bioactive TMJ disc implant, which aims to restore joint function, needs to be mechanically robust, enough to withstand joint loading during initial remodeling, and have a porosity that encourages cellular integration by improving mass transport conditions throughout the thickness of the scaffold.[25] The present study focused on the hypothesis that by utilizing CO_2 LMP a tunable microporosity can be designed into the natural scaffold to act as an artificial path for enhanced cell dispersion during seeding and mass transport during initial remodeling. Results show the LMP technique to improve cellular integration while maintaining the discs mechanical resilience over the 21-day culture period.

Materials and Methods

Dissection

Fresh porcine TMJ discs from male animals aged 6–9 months were purchased, with Institutional Animal Care and Use Committee (IACUC) approval (IACUC Protocol # 201207534) from Animal Technologies, Inc. (Tyler, TX). Dissection was conducted by first separating the mandible from the temporal bone, then ligaments connecting the disc to the condyle were detached, exposing the inferior disc surface (Fig. 1C). The remaining connections to the glenoid fossa were severed. Once removed, the mass and dimensions of each disc were measured and the superior surface and medial edge were marked using a water-resistant marker for ease of orientation during later regional sampling. Discs were stored in 0.15 M phosphate-buffered saline (PBS, pH 7.4) at 4°C for no more than 12 h before use.

Decellularization

TMJ discs were decellularized by immersion in a 1% SDS solution on an orbital shaker plate for 24 h at 100 rpm. Samples were then rinsed for 5, 15, and 30 min, followed by 1, 2, 4, 6, and 12 h in PBS (pH 7.4). Remaining DNA fragments were removed by incubation overnight (~8 h) at 37°C in 50 U/mL deoxyribonuclease (DNase) solution (Sigma-Aldrich, Inc., St. Louis, MO). Discs were then rinsed in PBS for 12 h and pH balanced to 7.3–7.4 before additional scaffold processing. To quantify residual SDS after rinsing and pH balancing, samples were evaluated using the Sigma-Aldrich Stains-All differential staining kit (Sigma-Aldrich, Inc.) comparing the final rinse solution to a standard SDS concentration in PBS curve, measured at 438 nm.[26] Decellularization of the TMJ discs was verified by the Quanti-iT PicoGreen assay as per the manufacturer's instructions (Invitrogen, Carlsbad, CA) to establish null DNA quantification (SDS treated) and verified visually by DAPI and calcein AM LIVE/DEAD Florescence Assay to visualize residual DNA (data not shown).

Lyophilization, LMP, and sterilization

Decellularized TMJ disc scaffolds were progressively frozen to −20°C for 6 h and then to −80°C for 18 h. After freezing, scaffolds were lyophilized (freeze-dried, Fig. 2E) for 24 h at −84°C in vacuum less than 8 mTorr (<1.66 Pa) using a benchtop freeze-drier (Millrock Technology, Kingston, NY). Once sublimation of the ice crystals was completed, the scaffolds were laser worked using a 40 W CO_2 laser engraver (Full Spectrum Laser, Las Vegas, NV). Holes were laser drilled with a 480 μm centerline-to-centerline separation distance in an 8×16 grid with a diameter of 120 μm, as illustrated in Figure 3A. A circular stainless steel punch (6 mm) was used to extract central zone samples

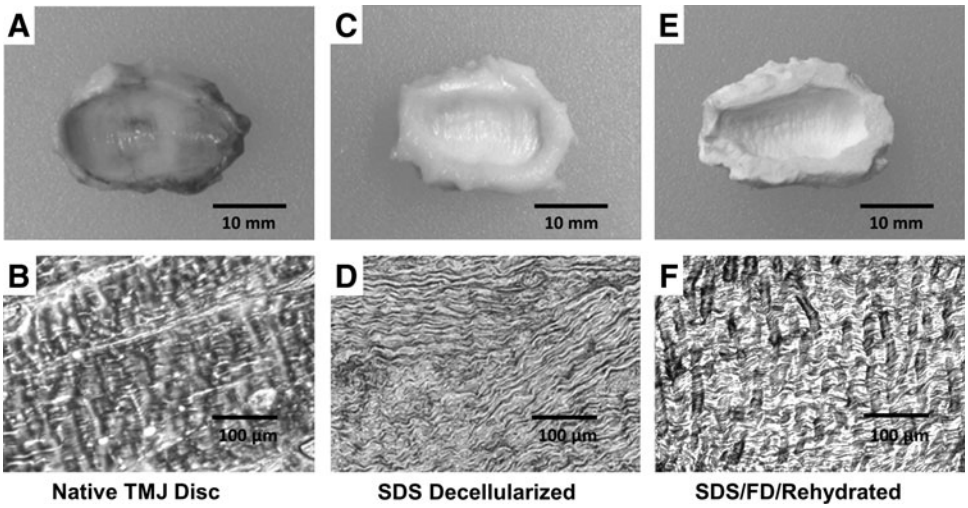

FIG. 2. Macrostructure and histological evaluation of detergent decellularization and lyophilization of TMJ disc. The native tissue has well-defined regional segmentation and very ordered extracellular matrix (ECM) fibril alignment, including well-defined collagen bundles **(A, B)**. The sodium dodecyl sulfate (SDS) decellularized disc macroscopically shows no pigmentation, and the microstructure has no evident cellular remnants; however, the ECM fibrils are compacted and irregularly aligned **(C, D)**. After the acellular scaffold is freeze-dried and rehydrated, the scaffold regains some of the native tissues fibril alignment's isometric quality and the individual ECM fibers have regained their collagen bundle conformation **(E, F)**.

(Fig. 3A, inset) and the superior surface marked for proper orientation during mechanical testing. Samples were then sterilized using the J. L. Shepherd Mark I, Model 35 research irradiator with a cesium 137 source and a dose of 12 kGy[27] at the University of Florida Nuclear Engineering Department. Scaffolds were stored under sterile conditions for at least 5 days to ensure any free energy from the sterilization process had dissipated before use.

Cell isolation and seeding

Wharton's Jelly-derived mesenchymal stem cells (MSCs) were isolated from human umbilical cord (hUC) Wharton's Jelly matrix. Full-term placental tissues were collected at the Shands Hospital Women's Delivery Ward (Gainesville, FL). Wharton's Jelly from the hUC was dissected and cut into 2- to 3-mm cubes and then cultured using the explant method to

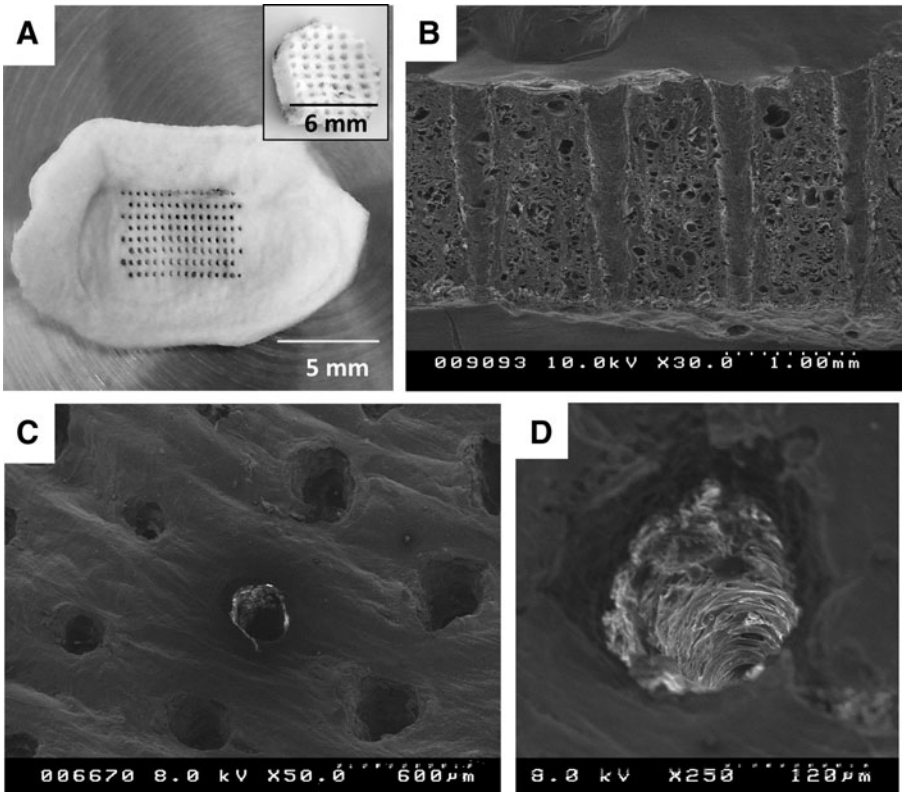

FIG. 3. Controllable uniformity of laser micropatterning (LMP) the TMJ disc scaffold. Scanning electron micrographs (SEMs) of the LMP TMJ disc illustrate that while there are minor (within experimental tolerances $\pm 50\,\mu m$) differences between hole diameters due to surface irregularities of the disc, the holes are uniformly spaced and traverse the thickness of the scaffold. **(A)** The pattern ablation into the whole TMJ disc tissue including an *inset* illustrating the LMP punch removed from the central region of the disc used for further evaluation. **(B, C)** Examination of the LMP holes via SEM. The SEMs illustrate that the surface of the TMJ disc is irregular, which causes cusping and burn rippling at the initial laser–tissue interaction. SEM of a single LMP hole ablated through the scaffold is shown in **(D)**.

isolate MSC. Explants and cells were cultured in complete media comprising Dulbecco's modified Eagle's medium (DMEM; Invitrogen) supplemented with 1% penicillin–streptomycin (Gibco Life Technologies, Grand Island, NY) and 10% fetal bovine serum (FetalPlex; Genimini Bio-Products, West Sacramento, CA) until passage-3 (p-3), with media being 100% replenished every 3 days. During passages, cells isolated from a number of cords are mixed and further cultured resulting in an MSC stock population. MSCs were inoculated with chondrogenic differentiation media 48 h before seeding at passage 3 (p-3) to drive the cells to differentiate into chondrocytes following the protocol developed by Wang *et al.*[28] Briefly, differentiation medium was composed of DMEM (Invitrogen) supplemented with 1% insulin-transferrin-selenium (Invitrogen), 0.1 nM dexamethasone (Sigma-Aldrich, Inc.), 10 mM ascorbic acid-2-phosphate (Sigma-Aldrich, Inc.), 1% penicillin–streptomycin (Gibco Life Technologies), 2% fetal bovine serum (FetalPlex; Genimini Bio-Products), 10 ng/mL of recombinant human epidermal growth factor (Sigma-Aldrich, Inc.), and 10 ng/mL of human platelet-derived growth factor BB (Sigma-Aldrich, Inc.).

Before seeding, freeze-dried samples were rehydrated for 6 h in standard culture media at 37°C in 48-well plastic culture plates. MSCs (p-3) were then seeded at a concentration of 900 cells per mm^2 in 1 mL of media onto the 6-mm-diameter scaffold punches that were sampled from the central zone of the disc. After 24 h, seeded scaffolds were transferred into 24-well TC plates and cultured for 7, 14, and 21 days under traditional culture conditions (5% CO_2 and 37°C) using complete media as described above.

Biomechanical analysis

A Biomomentum Mach1 Micromechanical System (Biomomentum, Inc. Laval, Quebec, Canada) was used for all mechanical testing. The testing chamber was filled with 0.15 M PBS (pH 7.4) to maintain hydration, similar to the *in vivo* environment,[29] and to maintain consistency with previous studies on TMJ tissue mechanics.[6,30] A stationary bottom plate and a vertically translating 2.5 cm diameter indenter of the Mach1 were used to generate the cyclic mechanical loading. Before testing, samples were allowed to equilibrate (unloaded) in PBS for 5 min at 37°C ± 1°C. Sample height was determined lowering the Mach1 indenter (rate of 0.005 mm/s) until a force of 0.0075 N was measured indicating sample contact with the indenter. This value was specified as the disc height.

The 6 mm central zone scaffold punches were compressed to 10% strain.[31,32] Vertical deformation (ΔL) required to produce this strain was calculated using the strain equation, $\varepsilon = \Delta L / L_0$ with the measured height (L_0) known from earlier measurement. The resulting compressive stress on each sample is defined by $\sigma = F_Z / A$, where F_Z is the compressive force and A is the cross-sectional area of the sample.[14] Resulting stress strain data averaged from loops 7 to 10 between 3% and 8% strain linear region were used to derive the steady-state compressive modulus (E) calculated from the equation $E = \sigma / \varepsilon$.

Hydraulic permeability

The ease of fluid flow through the porous sample was evaluated using a custom-built testing apparatus for hydraulic conductivity measurement. The device consisted of a two-chambered isolation setup with the TMJ disc scaffold punches acting as a permeable barrier between the two chambers. The two cylindrical chambers (internal volume, 2.5 cm^3) were vertically oriented such that the upper chamber when filled with fluid created a head pressure, which could be calculated at the beginning of the experiment.

The hydraulic permeability coefficient (k) was calculated from Darcy's Law, $k = \left(\frac{Q}{A}\right) / \left(\frac{\Delta P}{t}\right)$, where Q is the volumetric flow rate measured as the upper chambers internal volume divided by the time it took for the fluid to traverse the thickness of the scaffold, ΔP is the pressure difference across the sample at the start of the experiment, A is the permeation area of the sample (for our study the surface area of the 6 mm disc punch), and t is the thickness of the sample.

Cellular incorporation

Cellular adhesion was evaluated over the first 24 h of culture at time points 10 min, 2, 6, 12, and 24 h using the Quanti-iT PicoGreen assay as per the manufacturer's instructions (Invitrogen) after samples were frozen, cut into small sections, and degraded by overnight incubation in collagenase (Sigma-Aldrich, Inc.) in PBS at 37°C. Calibration curves were produced for known concentrations of cells to DNA that were then used to determine the DNA concentration/cell. At 2 and 24 h, the distribution of cell number was evaluated through the thickness of the sample by dividing the punch into three approximately equal segments with 0.60 ± 0.15 mm thickness (superior, mid, and inferior) and quantifying DNA content in each of these regions to approximate the uniformity of cell seeding through the thickness of the scaffold. DAPI and calcein AM LIVE/DEAD Florescence Assay were imaged at 24 h to illustrate seeding density of the disc scaffold and assess cell distribution and viability.

Metabolic activity (per cell) was assessed by quantifying the metabolic reduction of resazurin salts in media, against a calibration curve with a known concentration of cells of the same cell lineage. Briefly, culture media was supplemented with the nontoxic resazurin salt solution (1:10 salt solution to media concentration) and incubated with the construct for 2 h; then, the absorbance of the reduced resazurin was measured at wavelengths of 570 and 600 nm using a Synergy 2 microplate reader (BioTek, Winooski, VT). The relative metabolic activity in each sample related to the reduction or the resazurin molecule from oxidized (blue) form to reduced (red) form. Cellular metabolism was measured at 1, 7, 14, and 21 days in culture. Cellular metabolic activity was normalized against cell density, where the total metabolic activity of each sample was divided into the cell number.

Statistical analysis

Each set of test group data was calculated based on testing of nine samples ($n = 9$). Standard deviation and one-way analysis of variance (ANOVA) testing were used to determine statistical significance between test groups for biomechanics. Significance was established using the Tukey–Kramer test ($p = 0.05$, $n = 9$).

Results

The present study reports that modification of a decellularized TMJ disc by LMP enhances cellular infiltration

Table 1. Hydraulic Conductivity and Theoretical Permeability of the Native and Worked TMJ Disc Scaffold

	Hydraulic permeability coefficient (m^4/Ns)	*Compressive modulus (MPa)*	*% Hysteresis (last loop vs. initial loop)*
Native	1.79E–16 ± 0.04E–16	1.65 ± 0.24	64.00 ± 2.10
SDS decellularized	0.90E–16 ± 0.02E–16	3.49 ± 1.01	39.50 ± 6.70
SDS, FD, and rehydrated	1.26E–16 ± 0.31E–16	2.10 ± 0.65	71.70 ± 4.40
SDS, FD, 120 μm LMP	1.06E–16 ± 0.10E–16	2.20 ± 0.24	57.20 ± 5.50

Compressive fluid–solid properties of the TMJ scaffolds illustrate decreased hydraulic permeability coefficient for all processed scaffolds in comparison to native increased compressive modulus and altered energy dissipation capability. Extremes for all properties are observed after SDS decellularization and recovered toward native after freeze-drying and rehydration.

FD, freeze drying; LMP, laser micropatterning; SDS, sodium dodecyl sulfate; TMJ, temporomandibular joint.

through the 1.5- to 3-mm-thick dense matrix while not significantly altering biochemical and biomechanical properties from the native tissue. The LMP TMJ scaffold incorporated an artificial porosity, which acts to provide diffusion of nutrients and wastes to and from cells during initial remodeling.

Lyophilization and LMP of the TMJ disc scaffold

SDS decellularization and subsequent rinsing have been shown to effectively remove all cellular material.[14] Retention of SDS after PBS rinsing was evaluated and shown to be negligible using Sigma-Aldrich Stains-All differential staining kit (data not shown) (Sigma-Aldrich, Inc.). However, decellularization impacts the scaffold's ECM architecture by compacting the ECM fibers (Fig. 2B, D), resulting in an increase in the scaffold's compressive modulus and a decrease in the hydraulic permeability coefficient (Table 1). Histological inspection of the acellular scaffold after freeze-drying and rehydration illustrates that the ECM fibers swell and resemble the more isometric configuration of the native tissue (Fig. 2B, F). The recovery of fiber configuration occurs concurrently with the scaffold regaining its elastic quality after the initial stiffening resulting from SDS decellularization (Table 1). Figure 3A illustrates that the CO_2 40 W laser can produce repeatable organized microporosity, which traverses the thickness of the scaffold. Scanning electron micrograph (SEM) inspection of hole shape and alignment are within experimental tolerances (± 15 μm) despite the uneven surface layer (Fig. 3B). SEMs also show the ablations zones to have minimal thermal scouring (burning) around the hole (Fig. 3C). Representative stress-strain hysteresis in Figure 4 shows that an 8×16 grid of 120 μm holes has nominal effect on the compressive mechanics of the rehydrated tissue relative to native or control (SDS, freeze drying (FD), and hydrated/non-LMP) samples.

Cellular adhesion and regional seeding efficacy

Cellular adhesion to the LMP discs and control samples without LMP (non-LMP) 24 h after seeding are shown in Figures 5–7. Figure 5 illustrates the differences in total cell adhesion between LMP and non-LMP constructs throughout the initial 24 h of culture. Ten minutes after seeding, 63.68% of the total seeding concentration had adhered to the LMP scaffold, whereas the non-LMP cell adhesion was lower with 48.90% adhesion (16.24×10^3 cells/LMP scaffold vs. 12.47×10^3 cells/non-LMP scaffold, not statistical difference). From the initial seeding to 24 h of culture, both scaffolds experience significant loss in total cell adhesion with the LMP dropping to 51.21% of the total seeding

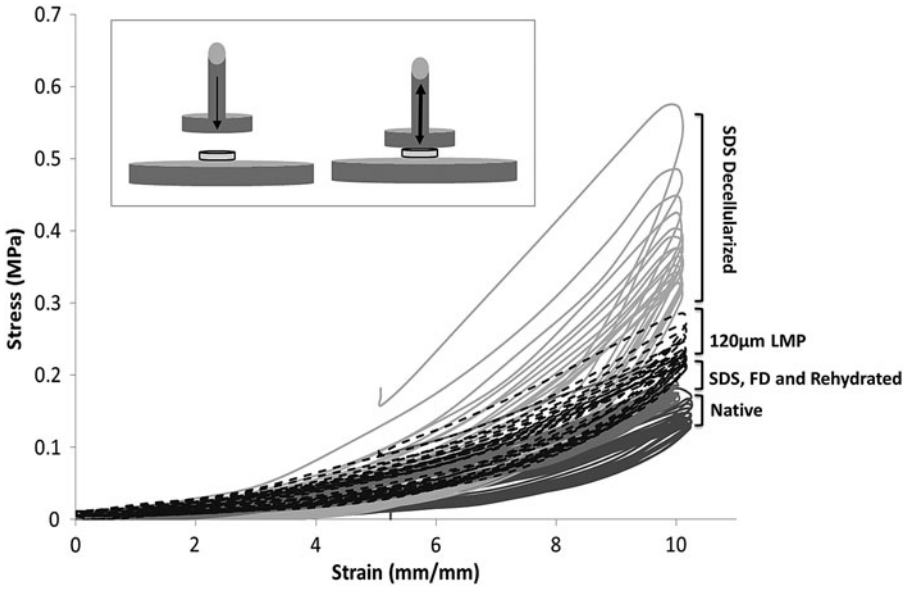

FIG. 4. Mechanical energy dissipation consequence of the scaffold processing technique. The mechanical ability of the TMJ disc at each stage of the scaffold processing technique was evaluated by cyclic compressive testing. Ten percent compressive strain was applied by a flat indenter and the resulting force was measured. From the force and surface area measured, the stress was calculated and is presented in this hysteresis. Higher stress and hysteresis are seen in the SDS decellularized tissue due to ECM protein conformational disruption by the highly ionic SDS molecule. Both stress and hysteresis recoup toward native properties after freeze-drying and rehydration. LMP of 120 μm pores increases stress marginally but does no increase hysteresis.

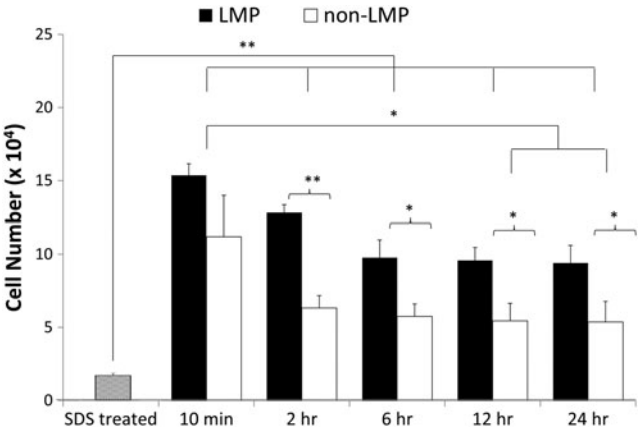

FIG. 5. Cell attachment over initial 24 h. Scaffolds were seeded with a density of 900 cells per mm^2 ($\sim$25,500 cells total/scaffold) and incubated at 5% CO_2 and 37°C for 10 min to 24 h and then evaluated for cellular concentration using the Quanti-iT PicoGreen assay. After 10 min, the LMP construct retained greater than 60% of cell seeding concentration and more than 80% of those cells remained adhered after the 24 h of incubation. The non-LMP scaffold, however, only retains about 45% of the 10 min cell density ($n=9$, $*p<0.05$, $**p<0.01$). Data for the SDS treated (null DNA criteria) are included and demonstrated statistical difference from all seeded samples.

concentration and the non-LMP retaining only 21.05% (13.07×10^3 cells/LMP scaffold vs. 5.37×10^3 cells/non-LMP scaffold, $**p<0.01$).

The uniformity of cellular adhesion through the thickness of the scaffold is shown in Figure 6, sections representing the superior, mid, and inferior zones of each construct are isolated and analyzed separately. DNA quantification results indicate that increased densities of cells adhere to surface zones (inferior and superior zones) of the LMP compared to the non-LMP constructs ($*p<0.05$ for all zones) and only LMP samples show the presence of cells in the mid zone 24 h after seeding. In Figure 7A and B, calcein AM florescence images illustrate that cells adhere at high densities to the surface of the naturally derived scaffolds. Adherent cells lay flat and extended adjacent to the surface ECM fibrils of the non-LMP scaffold, while cells adherent to the LMP scaffold have a less organized (anisotropic) orientation. DAPI and rhodomine phaloidin florescent staining of the scaffolds cross sections (Fig. 7C, D) show that cells of the LMP scaffold have adhered to the walls of the hole traversing the thickness of the scaffold, while cells are only localized on the scaffold periphery with the non-LMP samples.

Cellular integration and early remodeling

Cell proliferation data in Figure 8A show that the LMP samples had greater sustained cell proliferation and metabolic activity (per cell) compared to non-LMP constructs (cellular metabolism statistical difference between LMP and non-LMP constructs at all time points after day 1, $*p>0.05$, and day 21 cell number, $*p>0.05$). Cell density in the non-LMP constructs increased between day 7 and 14 (7.16×10^4 cells at day 7 to 15.83×10^4 cells, $**p>0.01$) followed by a steady-state population with no statistical difference in density, nor metabolic activity, through the remaining time course. The mechanical consequence of cellular integration through the thickness of the scaffold is illustrated in Figure 8B. Data show that the non-LMP scaffold exhibits linear geometric decrease in modulus with time. The LMP scaffold is significantly strengthened during initial cell incorporation (between day 1 and 7, $*p>0.05$) before eliciting typical scaffold mechanical weakening seen during static culture.

Histological sectioning seen in Figure 9 shows cellular migration from the pore periphery (initial adhesion site) into the scaffold and between LMP holes after 21 days in culture. Cell nuclei are apparent as far as 1000 μm from the edge of the sample and up to 235 μm from the edge of pattern holes (Fig. 9A, B). With non-LMP samples, no cell nuclei were present more than 500 μm from the sample edges (Fig. 9D, E). Only surface zones have high cell density in the non-LMP samples (Fig. 9D, E) and no cell populations are observed within the constructs interior. Both hematoxylin and eosin (H&E) and the florescent images show the ECM fiber alignment of the LMP scaffold has changed significantly

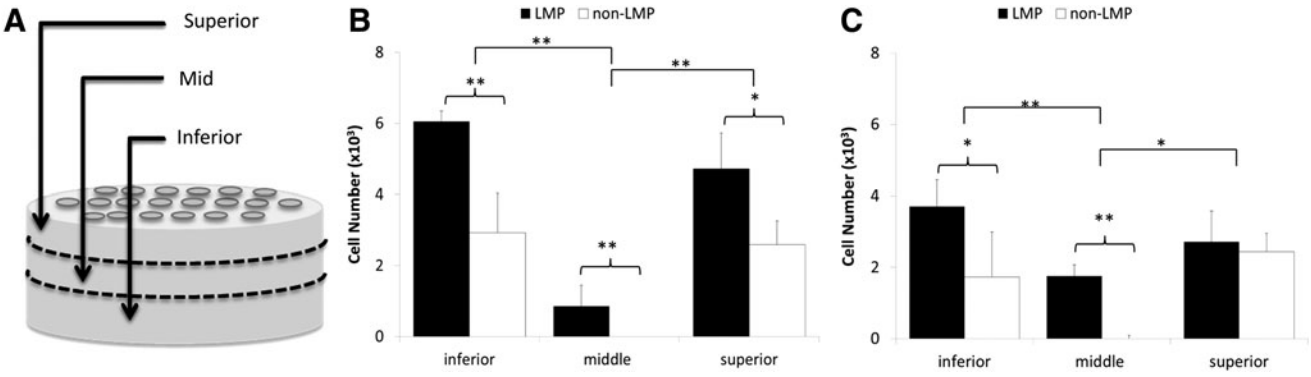

FIG. 6. Regional DNA quantification and cell seeding density as a function of thickness. **(A)** Cell adhesion was further evaluated by conducting DNA quantification with the Quanti-iT PicoGreen assay regionally from the superior surface through the scaffolds thickness at 2 h after seeding **(B)** and 24 h after seeding **(C)**. The analysis reveals that both the LMP and the non-LMP scaffolds retain a large cell population from seeding; however, the LMP scaffold has cell infiltration into the mid region of the tissue, identified in illustration **(A)**, while the non-LMP scaffold has no cell infiltration past the surface regions ($n=9$, $*p<0.05$, $**p<0.01$).

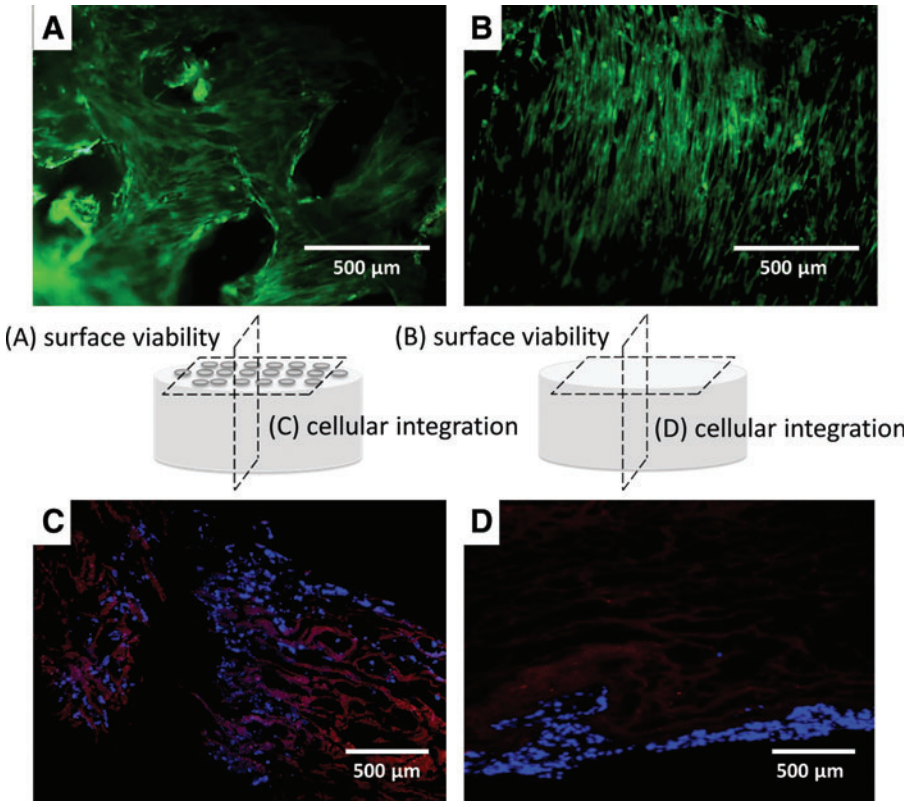

FIG. 7. Cellular attachment to the surface layer and through the cross section of the TMJ disc construct. Calcein-AM florescence staining of the *top* surface of the LMP **(A)** and non-LMP **(B)** scaffolds imaged 24 h after seeding shows that living cells have adhered and organized into a peripheral layer. DAPI staining identifies the nuclei of cells in cross-sectional histological slides taken at the centerline (3 mm from the edge) of both scaffolds **(C, D)**. The cross-sectional images clearly illustrate that the LMP scaffold have greater cellular adhesion because of the additional surface area the cells are exposed to, while the non-LMP scaffold has cell adhesion only at the periphery of the cross-sectioned sample. Color images available online at www.liebertpub.com/tea

from the initial adhesion architecture (Fig. 9A, B). Fibers are oriented anisotropically around the hole perimeter rather than oriented linearly as seen in the non-LMP scaffold.

Discussion

It has been previously stated that requirements to engineer a successful TMJ disc replacement are (i) a biodegradable or biocompatible scaffold with mechanical capability to withstand joint loading without fatigue or fragmentation; (ii) a representative cell source incorporating chondrocyte-like populations and fibroblast-like populations; (iii) suitable surface chemistry for cell attachment, proliferation, and differentiation; and (iv) cellular integration and microenvironment conducive to mass transport through the scaffold, as the native disc is primarily avascular and cells within the

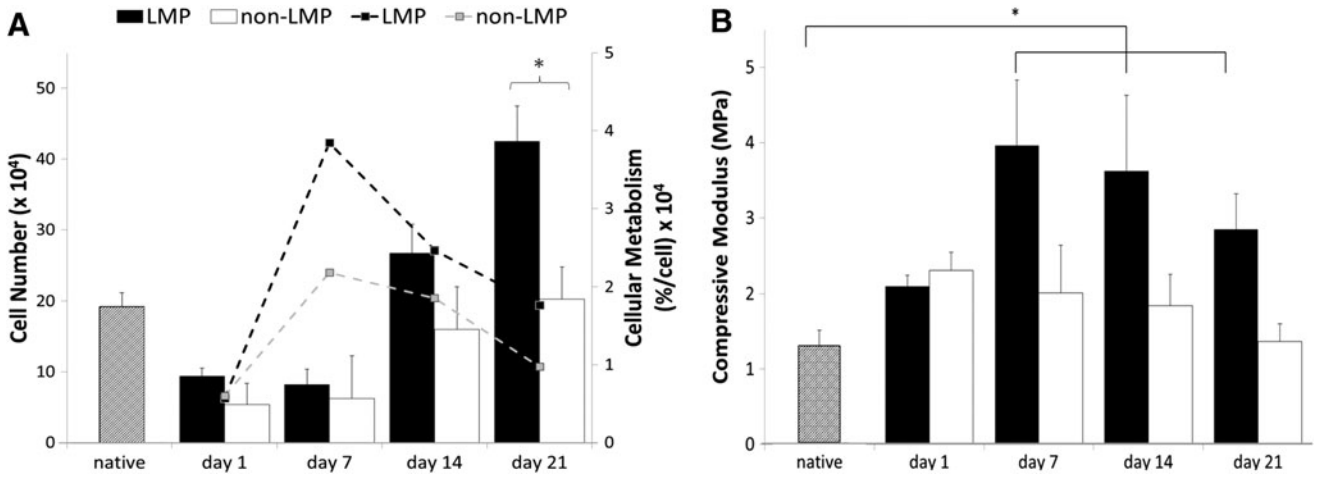

FIG. 8. Cellular proliferation and metabolism and mechanical characterization over the culture period. **(A)** Both the LMP and the non-LMP scaffolds show increase in cell number (bar graph) and cellular metabolism (dashed lines) during the culture period with the LMP scaffold exhibiting greater increases in both, likely due to higher initial cell adhesion because of the laser holes. **(B)** Compressive mechanical testing reveals that the compressive modulus of both the LMP and the non-LMP scaffolds at day 1 are comparable to the native disc properties. By day 7 of culture, the compressive properties of the LMP scaffold have significantly increased indicating a stiffening of the matrix; however, at day 14 and 21, the mechanical properties begin to decrease linearly similar to the non-LMP scaffold ($n=9$, $^*p<0.05$).

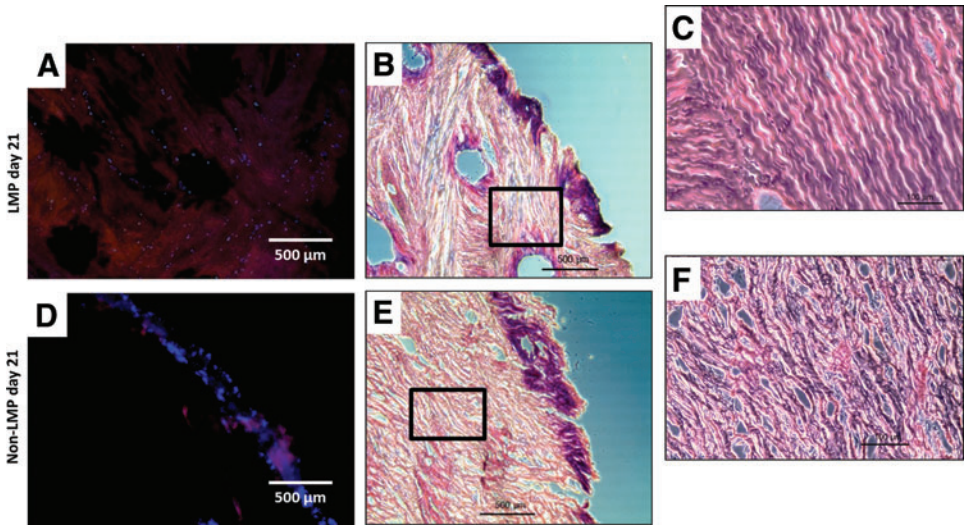

FIG. 9. Histological evaluation of culture at day 21. **(A, D)** DAPI/rhodamine phaloidin staining, illustrating that cellular presence within the constructs. **(B, E)** Hematoxylin and eosin (H&E) imaging at the same magnification as the florescence images and **(C, F)** are higher magnification sections of **(B, E),** respectively. **(A–C)** Cellular infiltration has spread between the LMP holes and has created a relatively uniform cell population, while **(D, E)** show that the non-LMP construct has only a dense layer of cells at the construct periphery and **(F)** shows no recognizable cells in the interior of the non-LMP construct. Sampling was taken from 500 μm from the superior surface of the samples for comparative consistency. Color images available online at www.liebertpub.com/tea

native disc receive glucose and oxygen from mechanical pumping of synovial fluid within the joint space.[33–35]

These works describe the application of a novel scaffold development addressing the hypothesis that incorporation of an artificial path of infiltration for cells, nutrients, wastes, oxygen, and other small molecules will improve a naturally derived acellular scaffold's potential for cellular integration and early remodeling capacity while retaining the native tissue's biochemical and biomechanical properties.

SDS decellularization to remove the tissue's native porcine cellular components, as well as other immunogenic epitopes, has been shown to maintain mechanical and biochemical properties comparable to native tissues.[14] The surfactant SDS decellularizes tissues by rupturing cell membranes through ionic disruption. Cell membranes, proteins, and cellular components as well as other soluble ECM components are surrounded and linearized by the highly charged SDS molecules and rinsed out of the scaffolding by diffusive gradients and agitation. However, higher concentrations of the surfactant solution induce secondary unwanted interactions with the insoluble components of the ECM. Figure 2B shows a light micrograph of the native TMJ ECM fiber orientation, and Figure 2D shows the TMJ scaffold after SDS decellularization. The structural effects resulting from SDS exposure on the fiber structure include linearization and loss of the crimped organization of the fibers. We hypothesized that the charged SDS molecules interact with collagen and elastin bundles by encapsulating them and destabilizing hydrogen and noncovalent bonds responsible for protein stability, tertiary and quaternary structure, causing the fibers to linearize.

The mechanical significance of this secondary interaction of SDS with the scaffold is shown in Table 1 and Figure 4. The SDS decellularization causes the compressive modulus to more than double from native value of 1.65–3.49 MPa and the representative hysteresis in Figure 4 illustrates that the acellular scaffold presents greater energy dissipated due to material deformation than the native tissue. The mechanical stiffening seen after SDS decellularization is in agreement with previous mechanical evaluations, on various tissue types, of the effects of SDS.[12,14,36,37] Interestingly, much of the mechanical consequence of this surfactant-based decellularization is recovered after the lyophilization step used to optimize the laser working of the scaffold; and again in Figure 2F, we observe correction of the ECM fibril conformation including the reorganization of the collagen aggregates (triple-helices fibrils). Our hypothesis postulates that after the PBS rinses most of the SDS molecules have been stripped from the scaffold ECM; however, the effects of the ionic surfactant remain (disruption to noncovalent bonds structuring the ECM microarchitecture). The lyophilization process involves sublimating frozen water crystals without modification to the microenvironment. During rehydration, water is drawn into the dried substance by capillary action and other hydration forces. We hypothesize that when water molecules are reintroduced some of the noncovalent bonds (specifically hydrogen bonds) are recovered via reorganization of aldol condensation for helical fibril organization. This process recovers a degree of the ECM fibrils correct conformation and in part restores the mechanical ability lost during decellularization.[38]

A constraint of many naturally based scaffolds is a consequence of the dense fibrous ECM networks with subcellular pore sizes that inhibit cell migration as well as limiting mass transport conditions. These limitations are exacerbated as populations increase further impeding cell migration, proliferation, ECM secretion, and remodeling. To circumvent these limitations, artificial pores were integrated into the acellular TMJ disc scaffold using a CO_2 laser. To optimize laser processing, decellularized discs were lyophilized

to eliminate laser diffraction within the hydrated scaffold. Figure 3 illustrates that lyophilization before laser patterning allows for the incorporation of uniform pores that traverse the full thickness of the scaffold. The mechanical consequence of these processing steps (decellularization, lyophilization, LMP, and rehydration) was evaluated using unconfined cyclic compressive loading with compressive modulus values presented in Table 1 and hysteresis in Figure 4. The mechanical ability of the LMP scaffold is within 5% of the control SDS decellularized FD and rehydrated scaffold and possesses energy dissipation trends similar to the native tissue, illustrating that our LMP scaffold has mechanical qualities comparable to the native disc.

Creation of a uniformly cell dense scaffold is imperative for fibrocartilage tissue engineering as the native tissue is largely avascular and nutrients are only obtained through diffusive mechanism; also pockets or zones of high cell density may result in hypoxia and inappropriate tissue regeneration during early remodeling events. Cell adhesion and retention was found to be improved with LMP constructs compared to nonpatterned constructs after 24 h of culture; however, initial adhesion was less than optimal with only 45% and 61% adhesion for non-LMP and LMP scaffold, respectively (Fig. 5). The more important finding from a construct developmental perspective is that cells were present throughout the thickness within LMP samples (Fig. 6B). Cell concentration within the mid layer of the scaffold proportionally increased relative to superior and inferior layers, which displayed a decrease in cellular presence between 2 and 24 h, while cell concentration of the LMP construct showed no statistical difference. This resulted in a near uniform cell distribution through the thickness of the 2.06 ± 0.26 mm LMP scaffold at 24 h (Fig. 6C). While the non-LMP scaffold shows a cell dense surface layer, no significant cellular infiltration was noted with DNA analysis (Fig. 6B, C) or by florescence imaging of the constructs cross section (Fig. 7D).

Construct development relies on the sequence of cellular adhesion, infiltration, colonization, and remodeling by metabolically active cells to synthesize an appropriate ECM. Metabolic activity of the cells within the constructs was evaluated at 1, 7, 14, and 21 days of culture. Both LMP and non-LMP scaffolds demonstrated an increase in metabolic activity of cells between day 1 and 7, likely a transition period in which the cells adhere and acclimate to the scaffolds initial ECM environment (Fig. 8A, dashed lines). Cells adhered to the LMP scaffold exhibit a greater than fourfold increase in the metabolic activity despite no significant increase in cell density over the initial 7 days of culture indicating that proliferation is secondary to stabilization within the natural matrix. The cell density quantified in the LMP constructs at days 14 and 21 were significantly higher than the non-LMP likely due to increased surface area and the availability of nutrients due to improved mass transport through the thickness of the scaffold.

The mechanical consequence of the constructs dense cellular repopulation is elucidated in the comparison of the LMP modulus against the non-LMP (Fig. 8B). The non-LMP constructs experience the typical mechanical degeneration over time as seen in unfixed natural matrix materials. The LMP scaffold experiences a mechanical strengthening before the degenerative trend is observed. The significant increase in elastic modulus seen only in the LMP scaffold and not the non-LMP constructs is a consequence of the laser working and more uniform cellular repopulation. As cells infiltrate a natural biopolymer, they secrete digestive enzymes and new matrix to cocoon themselves in an environment conducive to proliferation.[39] Cells seeded on the *ex vivo*-derived scaffolds used in these investigations would undergo very similar processes during initial culture (1–7 days), mildly interrupting the fibril alignment of the disc causing mechanical weakening of the ECM superstructure during early integration. Then, to a more significant consequence, filling the void space created by decellularization and laser ablation with their newly secreted matrix (Fig. 9). This occurs also in the non-LMP scaffold; however, only at the cell dense surface layer where direct interaction with culture media is possible.

Both constructs, the LMP and the non-LMP, exhibit the cell dense surface layer at 21 days of culture; however, observation of cellular presence through the thickness of the constructs after 21 days illustrated the continuity of cell distribution throughout the LMP construct, while cells on the non-LMP construct were limited to a periphery zone of only 200 ± 50 μm (Fig. 9). Finding increased cell populations within the interior of the LMP scaffold implies that a pore diameter of 120 μm is adequate to allow cell infiltration and adhesion without detachment due to fluid forces. Also that the pores are large enough that cells do not ''plug the hole'' during proliferation and limit nutrient transfer to and from cells within the constructs interior during initial remodeling.

Future studies will incorporate mechanical stimulation to encourage mechanotransduction of MSCs and guide matrix remodeling of the scaffolds superstructure. Moreover, further investigation of cellular enzymatic degeneration and ECM secretion will be imperative to develop conclusions about cell activity during early and extended remodeling events.

Conclusions

An ideal fibrocartilage scaffold for TMJ fibrocartilage disc replacement will exhibit a balance of biocompatibility, mechanical ability, and porosity.[40] The methodology described in these works develop a novel scaffold, which retains the mechanical resilience and biochemical microenvironment of the native TMJ disc and is augmented for cell adhesion and mass transport to support uniform cellular integration. These investigations prove that LMP into the natural ECM structure of the acellular TMJ improves the permeability of the dense ECM matrix scaffold. This improved permeability then supports uniform cellular integration and encourages cellular remodeling by providing a path of infiltration for metabolite diffusive action while not lessening the mechanical ability compare to the non-LMP. Early remodeling events are not inhibited by either the decellularization process or laser ablation but are accomplished with greater uniformity through the thickness of the scaffold. The techniques developed in these investigations can be applied to a multitude of naturally derived grafts as the LMP can be incorporated into thick whole tissue scaffolds (bone, ligament, cardiovascular, etc.) for direct implantation or further *in vitro* study.

Acknowledgments

We gratefully acknowledge the National Institutes of Health (NIH) National Institute of Dental and Craniofacial Research (1R21DE022449) for funding.

Disclosure Statement

This work is free of any conflicts of interest.

References

1. Nickel, J., and Mclachlan, K. An analysis of surface congruity in the growing human temporomandibular-joint. Arch Oral Biol **39,** 315, 1994.
2. Barbenel, J. Biomechanics of temporomandibular joint: theoretical study. J Biomech **5,** 251, 1972.
3. Naeije, M., and Hofman, N. Biomechanics of the human temporomandibular joint during chewing. J Dental Res **82,** 528, 2003.
4. Tanaka, E., and Koolstra, J. Biomechanics of the temporomandibular joint. J Dental Res **87,** 989, 2008.
5. Morel, V., Berutto, C., and Quinn, T. Effects of damage in the articular surface on the cartilage response to injurious compression *in vitro*. J Biomech **39,** 924, 2006.
6. Tanaka, E., Kawai, N., van Eijden, T., Watanabe, M., Hanaoka, K., Nishi, M., Iwabe, T., and Tanne, K. Impulsive compression influences the viscous behavior of porcine temporomandibular joint disc. Eur J Oral Sci **111,** 353, 2003.
7. Dolwick, M. Discectomy as an effective treatment for painful temporomandibular joint internal derangement: a 5-year clinical and radiographic follow-up. J Oral Maxillofac Surg **59,** 750, 2001.
8. Holmlund, A., Gynther, G., and Axelsson, S. Diskectomy in treatment of internal derangement of the temporomandibular-joint: follow-up at 1, 3, and 5 years. Oral Surg Oral Med Oral Pathol **76,** 266, 1993.
9. Ferreira, J., Ko, C., Myers, S., Swift, J., and Fricton, J. Evaluation of surgically retrieved temporomandibular joint alloplastic implants: pilot study. J Oral Maxillofac Surg **66,** 1112, 2008.
10. Beek, M., Koolstra, J., and van Eijden, T. Human temporomandibular joint disc cartilage as a poroelastic material. Clin Biomech (Bristol, Avon) **18,** 69, 2003.
11. Wilkes, C. Surgical-treatment of internal derangements of the temporomandibular-joint. A long-term study. Arch OtolaryngolHead Neck Surg **117,** 64, 1991.
12. Gilbert, T., Sellaro, T., and Badylak, S. Decellularization of tissues and organs. Biomaterials **27,** 3675, 2006.
13. McFetridge, P., Daniel, J., Bodamyali, T., Horrocks, M., and Chaudhuri, J. Preparation of porcine carotid arteries for vascular tissue engineering applications. J Biomed Mater Res A **70,** 224, 2004.
14. Lumpkins, S., Pierre, N., and McFetridge, P. A mechanical evaluation of three decellularization methods in the design of a xenogeneic scaffold for tissue engineering the temporomandibular joint disc. Acta Biomater **4,** 808, 2008.
15. Moore, M., Sarntinoranont, M., and McFetridge, P. Mass transfer trends occurring in engineered *ex vivo* tissue scaffolds. J Biomed Mater Res A **100,** 2194, 2012.
16. Francis, K., and Palsson, B. Effective intercellular communication distances are determined by the relative time constants for cyto/chemokine secretion and diffusion. Proc Natl Acad Sci U S A **94,** 12258, 1997.
17. Vogel, A., and Venugopalan, V. Mechanisms of pulsed laser ablation of biological tissues (vol 103, pg 577, 2003). Chem Rev **103,** 2079, 2003.
18. Brugmans, M., Kemper, J., Gijsbers, G., Vandermeulen, F., and Vangemert, M. Temperature response of biological-materials to pulsed non-ablative co2-laser irradiation. Lasers Surg Med **11,** 587, 1991.
19. Murphy, C., Haugh, M., and O'Brien, F. The effect of mean pore size on cell attachment, proliferation and migration in collagen-glycosaminoglycan scaffolds for bone tissue engineering. Biomaterials **31,** 461, 2010.
20. O'Brien, F., Harley, B., Yannas, I., and Gibson, L. The effect of pore size on cell adhesion in collagen-GAG scaffolds. Biomaterials **26,** 433, 2005.
21. Melchels, F., Barradas, A., van Blitterswijk, C., de Boer, J., Feijen, J., and Grijpma, D. Effects of the architecture of tissue engineering scaffolds on cell seeding and culturing. Acta Biomater **6,** 4208, 2010.
22. Maidhof, R., Marsano, A., Lee, E., and Vunjak-Novakovic, G. Perfusion seeding of channeled elastomeric scaffolds with myocytes and endothelial cells for cardiac tissue engineering. Biotechnol Prog **26,** 565, 2010.
23. Daskalova, A., Bashir, S., and Husinsky, W. Morphology of ablation craters generated by ultra-short laser pulses in dentin surfaces: AFM and ESEM evaluation. Appl Surf Sci **257,** 1119, 2010.
24. Lee, B., Jeon, H., Wang, A., Yan, Z., Yu, J., Grigoropoulos, C., and Li, S. Femtosecond laser ablation enhances cell infiltration into three-dimensional electrospun scaffolds. Acta Biomater **8,** 2648, 2012.
25. Place, E., Evans, N., and Stevens, M. Complexity in biomaterials for tissue engineering. Nat Mater **8,** 457, 2009.
26. Rusconi, F., Valton, E., Nguyen, R., and Dufourc, E. Quantification of sodium dodecyl sulfate in microliter-volume biochemical samples by visible light spectroscopy. Anal Biochem **295,** 31, 2001.
27. Vangsness, C., Triffon, M., Joyce, M., and Moore, T. Soft tissue for allograft reconstruction of the human knee: a survey of the American Association of Tissue Banks. Am J Sports Med **24,** 230, 1996.
28. Wang, L., Seshareddy, K., Weiss, M., and Detamore, M. Effect of initial seeding density on human umbilical cord mesenchymal stromal cells for fibrocartilage tissue engineering. Tissue Eng Part A, **15,** 1009, 2009.
29. Piette, E. Anatomy of the human temporomandibular joint. An updated comprehensive review. Acta Stomatol Belg **90,** 25, 1993.
30. Allen, K., and Athanasiou, K. Viscoelastic characterization of the porcine temporomandibular joint disc under unconfined compression. J Biomech **39,** 312, 2006.
31. Juran, C., Dolwick, M., and McFetridge, P. Shear mechanics of the TMJ disc: relationship to common clinical observations. J Dental Res **92,** 193, 2013.
32. Kim, K., Wong, M., Helfrick, J., Thomas, J., and Athanasiou, K. Biomechanical tissue characterization of the superior joint space of the porcine temporomandibular joint. Ann Biomed Eng **31,** 924, 2003.
33. Almarza, A., and Athanasiou, K. Design characteristics for the tissue engineering of cartilaginous tissues. Ann Biomed Eng **32,** 2, 2004.
34. Detamore, M., and Athanasiou, K. Motivation, characterization, and strategy for tissue engineering the temporomandibular joint disc. Tissue Eng **9,** 1065, 2003.

35. Kuo, J., Shi, C., Cisewski, S., Zhang, L., Kern, M., and Yao, H. Regional cell density distribution and oxygen consumption rates in porcine TMJ discs: an explant study. Osteoarthritis Cartilage **19,** 911, 2011.
36. Gratzer, P., Harrison, R., and Woods, T. Matrix alteration and not residual sodium dodecyl sulfate cytotoxicity affects the cellular repopulation of a decellularized matrix. Tissue Eng **12,** 2975, 2006.
37. Reing, J., Brown, B., Daly, K., Freund, J., Gilbert, T., Hsiong, S., Huber, A., Kullas, K., Tottey, S., Wolf, M., and Badylak, S. The effects of processing methods upon mechanical and biologic properties of porcine dermal extracellular matrix scaffolds. Biomaterials **31,** 8626, 2010.
38. Prestrelski, S., Tedeschi, N., Arakawa, T., and Carpenter, J. Dehydration-induced conformational transitions in proteins and their inhibition by stabilizers. Biophys J **65,** 661, 1993.
39. Blackwoo, H.J. Cellular remodeling in articular tissue. J Dental Res **45,** 480, 1966.
40. Xie, J., Ihara, M., Jung, Y., Kwon, I., Kim, S., Kim, Y., and Matsuda, T. Mechano-active scaffold design based on microporous poly(L-lactide-co-epsilon-caprolactone) for articular cartilage tissue engineering: dependence of porosity on compression force-applied mechanical behaviors. Tissue Eng **12,** 449, 2006.

Address correspondence to:
Peter S. McFetridge, PhD
J. Crayton Pruitt Family
Department of Biomedical Engineering
University of Florida
JG-56
Biomedical Sciences Building
Gainesville, FL 32611-6131

E-mail: pmcfetridge@bme.ufl.edu

Received: May 1, 2014
Accepted: September 19, 2014
Online Publication Date: January 8, 2015